Tailored Solution-Based *N*-heterotriangulene Thin Films: Unravelling the Self-Assembly

Tim Hawly,[a] Fabian Streller,[a] Manuel Johnson,[a] Sandra Miguez-Lago,[b] Natalie Hammer,[b] Frank Hampel,[b] Dustin Vivod,[c] Dirk Zahn,[c] Milan Kivala,[d] Robert Branscheid,[e] Erdmann Spiecker,[e] and Rainer H. Fink*[a]

The ability of a series of bridged triarylamines, so-called *N*-heterotriangulenes, to form multilayer-type 2D-extended films via a solution-based processing method was examined using complementary microscopic techniques. We found that the long-range order, crystallinity, and layer thickness decisively depend on the nature of the substituents attached to the polycyclic backbone. Owing to their flat core unit, compounds exhibiting a carbonyl unit at the bridge position provide a superior building block as compared to thioketone-bridged derivatives. In addition, nature and length of the peripheral substituents affect the orientation of the aromatic core unit within highly crystalline films. Hence, our results stress the significance of a suitable molecular framework and provide deeper understanding of structure formation in 2D-confined surroundings for such compounds.

1. Introduction

In the past three decades, organic semiconductors (OSCs) have emerged as a viable, low-cost and environmentally friendly alternative to amorphous hydrogenated silicon-based circuitry in modern microelectronics such as radio frequency identification tags, wearable electronics or sensors.[1–3] While conventional inorganic devices are to a certain extent limited to rigid substrates, an appealing advantage of organic electronics resides in its compatibility with flexible and elastic supports such as polymers while still being lightweight or, depending on the target application, even transparent.[3–5] Accordingly, first functional OSC layers in the 1980s also consisted of polymeric materials such as polyacetylene[6] or polythiophene.[7] However, it quickly became obvious that charge transport along such junctions is severely hampered by the intrinsic disorder of the long-chained backbone structures.[8] Therefore, reduction of grain boundaries acting as charge traps and simultaneous establishment of a high degree of molecular order is widely considered as the decisive challenge towards efficient charge transport in up-to-date OSC films.[9–12] Consequently, special emphasis is placed on the introduction of sufficient intermolecular interactions such as effective π-π-stacking and hydrophobic interactions to yield a highly crystalline microstructure. For instance, the contribution of elongated alkyl chains attached to a core unit is thought to benefit the interaction and hence, the electronic coupling of π-electron-rich molecular sections with increasing chain length, *i.e.* they act as a molecular fastener as a result of their intermolecular cooperative van-der-Waals (VDW) interactions.[13–16] As a result, charge-carrier mobilities within functional 2D layers of organic electronics have improved considerably and remain the key to success for devices such as organic light-emitting diodes (OLEDs) and organic field-effect transistors (OFETs).[17–20]

Numerous powerful hole-transporting (p-type) OSCs such as pentacene derivatives[21,22] or thiophene-based[5,13,23] small molecules have found their way into cutting-edge applications due to their solution processability and high stability under both atmospheric conditions and elevated temperatures.[24–26] Their straightforward synthetic modifiability allows for tailor-made molecular structures that are capable to significantly reduce molecular disorder.[27,28] In contrast to that, efficient charge-carrier transport through electron-deficient (n-type) junctions remains challenging, yet indispensable in complementary logic

[a] T. Hawly, F. Streller, M. Johnson, Prof. Dr. R. H. Fink
Friedrich-Alexander-Universität Erlangen-Nürnberg
Chair of Physical Chemistry II
Egerlandstraße 3
91058 Erlangen, Germany
E-mail: rainer.fink@fau.de

[b] Dr. S. Miguez-Lago, Dr. N. Hammer, Dr. F. Hampel
Friedrich-Alexander-Universität Erlangen-Nürnberg
Chair of Organic Chemistry I
Nikolaus-Fiebiger-Str. 10
91052 Erlangen, Germany

[c] D. Vivod, Prof. Dr. D. Zahn
Friedrich-Alexander-Universität Erlangen-Nürnberg
Chair of Theoretical Chemistry
Nägelsbachstraße 25
91052 Erlangen, Germany

[d] Prof. Dr. M. Kivala
Ruprecht-Karls-Universität Heidelberg
Institute of Organic Chemistry & Centre of Advanced Materials
Im Neuenheimer Feld 270 & 225
69120 Heidelberg, Germany

[e] R. Branscheid, Prof. Dr. E. Spiecker
Institute of Micro- and Nanostructure Research & Center for Nanoanalysis and Electron Microscopy (CENEM), Friedrich-Alexander-Universität Erlangen-Nürnberg, IZNF
Cauerstraße 3, 91058 Erlangen, Germany

Supporting information for this article is available on the WWW under https://doi.org/10.1002/cphc.202100164

ChemPhysChem

Articles
doi.org/10.1002/cphc.202100164

Chemistry
Europe
European Chemical
Societies Publishing

circuits.[24,29–31] The comparably rather slow development of effective n-type OSCs is mainly a result of the instability of radical anions, *i.e.*, the transferred charge carrier, in the presence of oxygen or moisture.[32,33]

In addition, the commonly large injection barrier between the work function of common electrode metals and the lowest unoccupied molecular orbital (LUMO) of the respective semiconductor interferes with efficient charge transport through n-type junctions.[29] Despite the fact that traditionally the synthetic challenge of attaching electron deficient functional groups to π-conjugated cores is higher as compared to electron donating moieties, successful synthetic approaches have been reported recently.[29,34,35]

Herein, we focus on both the synthesis of novel, particularly functionalized *N*-heterotriangulene molecules as well as their capability to form well-oriented, two-dimensional films and, most importantly, potential n-type systems upon solution processing.[36–39] The synthesis of core unit **1** (Figure 1) was based on a procedure first reported by Chen and coworkers.[40] Bridging the aryl moieties through the *ortho* positions with respect to the central nitrogen atom accounts for planarization of the originally propeller-shaped triphenylamine moiety.
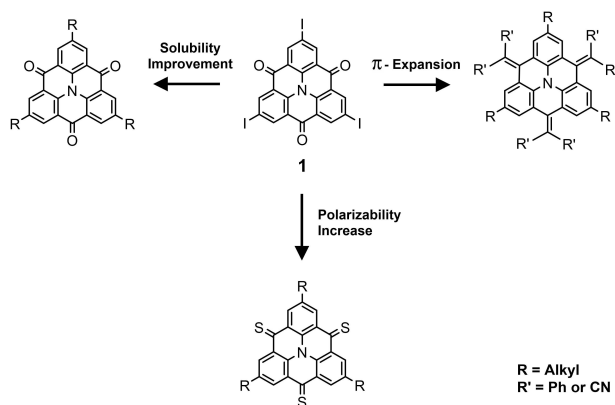

Figure 1. Possible pathways towards tailor-made *N*-heterotriangulenes based on compound **1**.
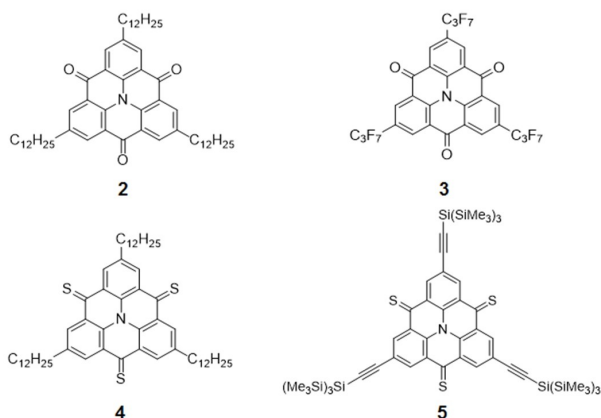

Figure 2. Functionalized *N*-heterotriangulenes examined.

Consequently, the resulting nitrogen-centered scaffold is susceptible to triple lateral functionalization. Besides the necessity of exchanging the halide substituents at the aryl *para*-positions with alkyl chains to enhance solubility in common organic solvents, which was namely accomplished by Negishi (**2** and **4**), Ullmann (**3**), and Sonogashira (**5**) cross-couplings, the π-system can also be extended at the bridge positions or the carbonyl oxygen replaced by more polarizable sulfur atoms via Lawesson's reagent treatment (see SI1 and SI2 for synthetic details and characterization data).

It should be noted that other rigid, π-conjugated electron deficient *N*-heterotriangulenes have been investigated before[41] and especially compound **2** (Figure 2) has already been discussed by Müllen and coworkers regarding both its solution processability and the crystal structure in columnar (1D) thin films from a dip-coating approach.[42] With respect to compounds **2**, **4** and **5**, we anticipate molecular fragmentation at elevated temperatures due to the long-chained moieties at the periphery and/or the rather unstable C=S unit at the backbone. This eliminates vacuum sublimation as a straightforward deposition technique for these molecules.[43–45] Therefore, we focus on the realization of extended 2D systems via a solution-based approach coined "solution-epitaxy" initially reported by Hu and coworkers.[46] Here, the solvent-water interface is utilized as a potentially defect-free substrate supporting molecular self-assembly (see experimental section for details). As opposed to conventional film deposition techniques such as thermal evaporation or dip coating, self-organization takes place close to equilibrium conditions *en route* to highly ordered 2D systems. Still, we expect to overcome the characteristic drawback of diffusion-controlled growth *in vacuo* and realize well-structured and potentially crystalline films in the mm² range in solution.[46,47] We did not consider compression of the floating molecules comparable to the realization of Langmuir-type systems due to the lack of amphiphilic character of the utilized compounds.

2. Results

All *N*-heterotriangulenes discussed herein possess good solubility in common organic solvents such as dichloromethane, chloroform, toluene, and acetonitrile and hence constitute ideal frameworks for self-assembly at the liquid-liquid interface in the concentration range between 0.025–0.5 mg/mL. Compounds **2**, **3** and **5** account for long-range formation of closed film structures, while **4** appears to be closed only to the naked eye as optical microscopy (OM) reveals a discontinuous microstructure composed of numerous flake-like agglomerates. Interestingly, the sole difference in molecular structure as compared to **2** is the replacement of oxygen at the bridge positions by more polarizable sulfur atoms, yet the resulting film structure is inherently different (Figure 3c). It is noted that for the conventionally used 0.25 mg/mL original solution concentration, no isotropic, 2D-confined growth behavior is observed for compound **4**. Moreover, both carbonyl-bridged compounds **2** and **3** exhibit a preferred in-plane growth
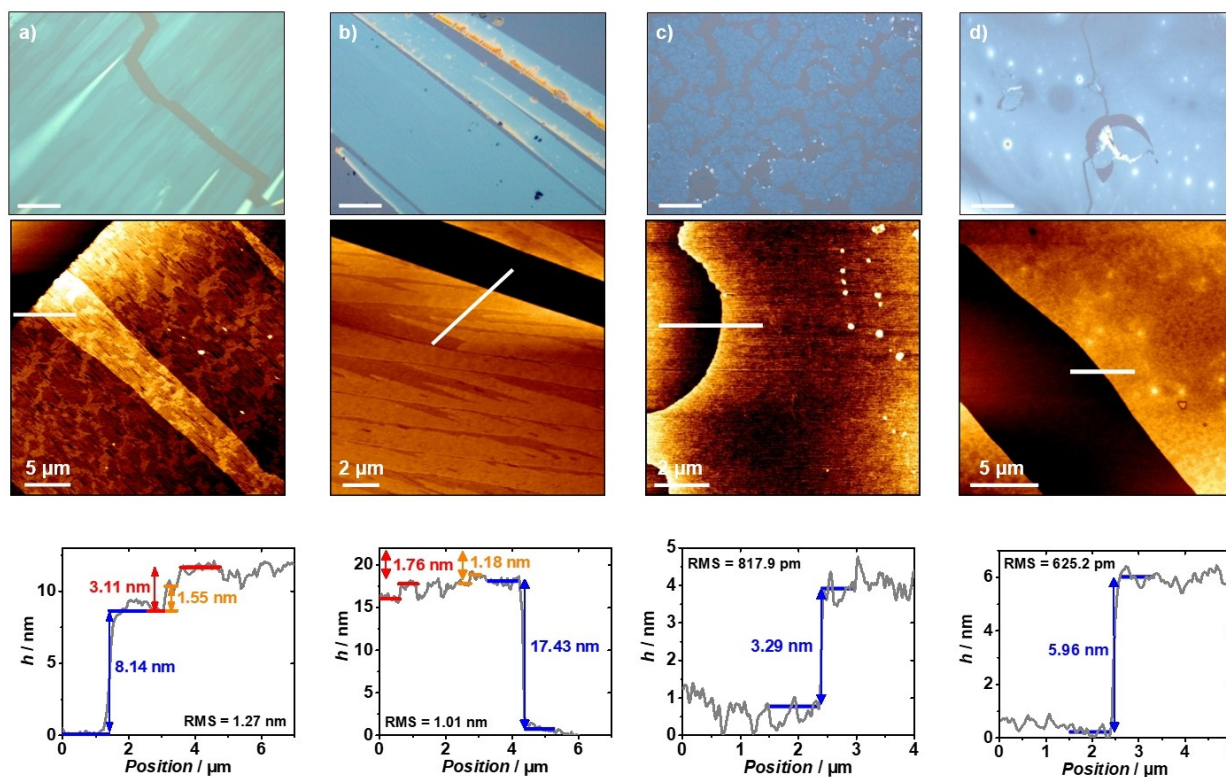
ChemPhysChem

Articles
doi.org/10.1002/cphc.202100164

Chemistry Europe
European Chemical
Societies Publishing

Figure 3. OM (top) and non-contact mode AFM images (bottom) with corresponding height profiles for N-heterotriangulene thin films based on a) 0.25 mg/mL chloroform/toluene (2:1) solution of **2**, b) 0.25 mg/mL chloroform solution of **3**, c) 0.0625 mg/mL dichloromethane solution of **4** and d) 0.25 mg/mL chloroform solution of **5**. In all OM images the scalebar corresponds to 100 μm.

direction observable neatly via OM (Figure 3a,b). Cracks within the microstructure disrupting the continuous thin film (Figure 3a,d) are most likely caused by the introduction of mechanical stress into the few-layer systems during the transfer procedure from the water surface onto the silicon oxide substrate.

The overall film morphology and thickness is determined via non-contact atomic force microscopy (AFM) at the above-mentioned film disruptions as depicted for compounds **2** and **3** within Figure 3. We observe a base film thickness of 8.14 nm (Figure 3a) and 17.43 nm (Figure 3b) respectively. On top of these initial structures, additional layered structures are distinguishable corresponding to 2D-extended agglomerations of the respective compounds. Taking the maximum molecular extension of **2** (3.79 nm) and **3** (1.52 nm) into account, the dimension of such step-like structures hints towards monomolecular layers or – assuming a lying-down configuration – also bimolecular layers on top of the thicker base film (line profiles within Figure 3a,b). It is noted that the long, flexible dodecyl chains attached to **2** in order to increase the solubility should still be flexible in the solid state and hence, the morphology appears to be rather rough (RMS roughness value = 12.7 Å).

Moreover, narrow drawn-out crevices are found in the film morphology of **2**, which can be explained by toluene being one of the components in the original solution. As an aromatic solvent, toluene may participate in the π-π stacking events

between the core units during structure formation and hence, accumulate within the film. This is also supported by AFM images of compounds **3–5**, which are not based on toluene containing solution and thus, lack such features. After deposition onto the solid support, the remaining solvent is expected to gradually evaporate from the film leading to minor gaps, which, with respect to the layer surface, are around 2.5 nm deep.

Thin films of **3** similarly show distinct directional growth behavior, however, the base film thickness is almost twice as high as for **2**. As a result of this and due to the perfluorinated n-propyl chains being significantly shorter than the dodecyl chains of **2**, we observe a considerably smaller surface roughness of only 10.1 Å. Upon replacement of the carbonyl bridging moieties with thiocarbonyls, a preferential growth direction is no more observed. Interestingly, film formation appears to be limited to the base film on the water surface with a thickness of only 3.29 nm (**4**, Figure 3c) and 5.96 nm (**5**, Figure 3d), respectively. This corresponds to only a few molecular layers depending on the exact molecular orientation within the films. Simultaneous to its oxygen-containing derivative, the dodecyl chains of **4** account for a larger RMS value of 8.2 Å as compared to the bulkier, yet significantly shorter acetylene–Si(SiMe$_3$)$_3$ groups of **5** (RMS roughness value = 6.3 Å). In contrast to carbonyl-bridged N-heterotriangulene thin films of **2** and **3**, continuous layered growth is not observed within thiocarbonyl-

ChemPhysChem

Articles
doi.org/10.1002/cphc.202100164

Chemistry
Europe
European Chemical
Societies Publishing

bridged compounds, which lack consistent structure formation beyond the ultrathin base film. As the film surface lacks molecular steps, a considerably lower roughness is observed for both **4** and **5**. This leads us to the conclusion that chain length is more decisive regarding the film roughness than the bulkiness of the substituents attached to the aryl *para*-positions of the core unit.

To obtain a more detailed insight into the microstructure and molecular orientation within the prepared organic thin films, angle dependent near-edge X-ray absorption fine structure (NEXAFS) measurements were carried out for all four compounds. The absorption intensity of distinct electronic transitions from core levels (C1s) into unoccupied molecular orbitals was recorded ranging from grazing incidence angles ($\theta = 20°$) to normal incidence ($\theta = 90°$) using photons that are polarized in the plane of incidence (p-polarization). In general, the absorption intensity, I_v, is then given by (1)[48,49] with θ being the experimental photon incidence angle (with respect to the film surface), α being the polar angle (with respect to the rotational axis defining θ) and φ being the azimuthal angle (with respect to the plane of incidence).

$$I_v = cos^2\theta\ cos^2\alpha + sin^2\theta\ sin^2\alpha\ cos^2\varphi$$
$$+ 2\ sin\ \alpha\ cos\ \alpha\ sin\ \theta\ cos\ \theta\ cos\ \varphi \qquad (1)$$

The direction of the final state orbital is described by both the polar angle between the surface normal and the final state orbital α, and the azimuthal angle φ. In particular, the lower energetic C1s→π*-transitions contain valuable information

regarding the orientation of the rigid aromatic backbone of all four compounds with respect to the substrate. Once a preferential average orientation within the specimen is apparent and α is larger than the 'magic angle' of 54.7°, the strength of the absorption peak resulting from the lower energetic π*-transition rises with θ and the strength of the higher energetic σ*-transition decreases accordingly (linear dichroism effect).[49] This is because both orbitals are perpendicular to each other with the trend being reversed for $\alpha < 54.7°$. Accordingly, qualitative information can be gathered regarding a preferential, *i.e.*, potentially crystalline, orientation within the thin film. For highly aligned films and considering twofold and higher substrate symmetry,[48,49] we may also deduce the azimuthal angle φ according to

$$I_v = cos^2\theta\ cos^2\alpha + sin^2\theta\ sin^2\alpha\ cos^2\varphi \qquad (2)$$

Here, C K-edge spectra recorded for compounds **2** and **3** both show significant dichroic effects (Figure 4c,d), *i.e.*, preferential molecular orientation exists within the examined film areas. For compound **2**, the region from 284 eV to approximately 287 eV is assigned to low-energy π*-resonances of the various carbon double bonds in the core unit (Figure 4a).[48,50–53] Although the absorption intensity for the π*(C=C)-transitions varies depending on the photon incidence angle to some extent, intensity changes in the spectrum occur in an unambiguous fashion (see SI3-1 for intermediate values of θ and additional spectra). In accordance, π*-transitions arising from the three nitrogen-bound aromatic C-atoms ($E_{Ph} =$
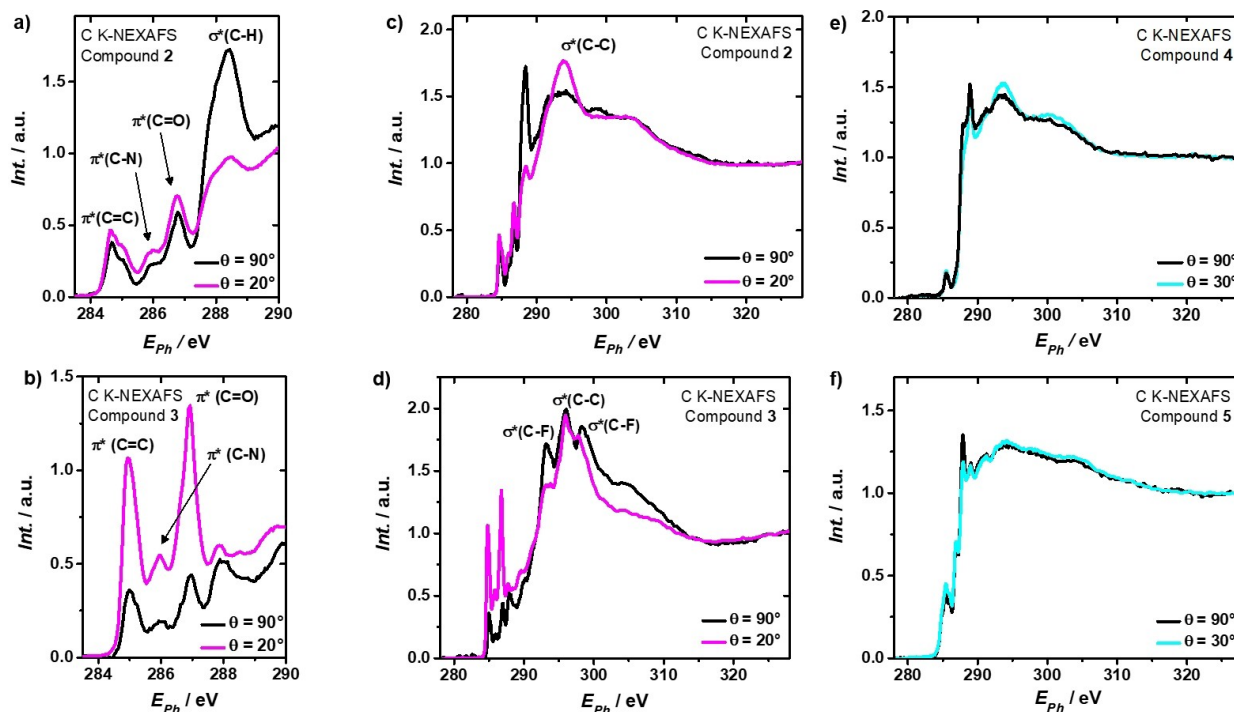

Figure 4. Normalized angle-dependent NEXAFS spectra for *N*-heterotriangulenes **2–5**. Significant resonant energies at glancing and normal incidence within the edge jump region are shown for a) compound **2** and b) compound **3**. Full-range spectra are depicted within c) compound **2**, d) compound **3**, e) compound **4** and f) compound **5**.

ChemPhysChem

Articles
doi.org/10.1002/cphc.202100164

Chemistry Europe
European Chemical
Societies Publishing

286 eV),[54,55] and the three carbonyl moieties ($E_{Ph} = 286.8$ eV)[56] show similar absorption behavior for normal and grazing incidence. This is due to the respective unoccupied orbitals also belonging to the rigid and planar *N*-heterotriangulene core unit. The distinct sharp band at ~288.4 eV within the estimated edge jump region is related to the dominating σ*(C–H)-transitions of the saturated dodecyl chains explaining its strong intensity as compared to the low-energetic π*-resonances.[57,58]

Qualitatively, this resonance has the strongest intensity when $\vec{E}$ is oriented perpendicular to the backbone of the dodecyl chain, *i.e.*, $\vec{E}$ lies within the CH$_2$ plane ($\theta = 90°$).[59] Quantitative analysis (Figure 5a, see also SI3-1) of the angle-dependent absorption intensity using the σ*-(CH)-resonance at 288.4 eV yields an average σ*-orbital tilt angle of $\alpha = 72 \pm 2°$ with respect to the surface normal. As a result, the C$_{12}$-substituents of **2** are close to standing upright in the film. This is further supported by the weak absorption intensity at 293.3 eV, which is ascribed to the σ*(C–C)-transition of the chain backbone (Figure 4c),[60] at $\theta = 90°$ and opposite behavior at grazing incidence ($\theta = 20°$). Regarding the orientation of the *N*-heterotriangulene backbone, we anticipate the π*-orbital polar angle α to be in the regime of the magic angle of 54.7°, which explains the small intensity changes in the π*-region upon rotation around θ.[48,49] This also implies that the plane of the core unit within the microscopically well-defined film should be tilted around 35° from the surface normal (Table 1).

NEXAFS spectra of **3** (Figure 4b,d) reveal a large overall absorption intensity for the sharp, pre-edge π*-transitions compared to the broader, post-edge σ*-transitions, regardless of the experimental photon incidence angle, θ. This is due to the perfluorinated n-propyl chains being much shorter than the alkyl substituents of **2**, **4** and **5**. Accordingly, their lower contribution to the total absorption intensity of the molecule emphasizes the contribution of the π-rich core unit in this part of the spectrum. The observed resonant transitions resemble

those present for compound **2**, which is to no surprise as both molecules share the same backbone. The strong dichroic behavior within the lower energetic part of the spectrum (Figure 4b) indicates a π*-orbital tilt angle of $\alpha < 54.7°$ from the surface normal. Within the σ*-region, resonances at 292.1 eV, 298.3 eV (attributed to CF$_2$ and CF$_3$ transitions, respectively) and 296.1 eV (C–C transition) assignable to the perfluorinated chains show varying intensity for both incidence angles (Figure 4d, see SI3-2), confirming a preferential molecular orientation. This specific change in absorption intensity, *i.e.*, a strong C–F absorption and weak C–C absorption at normal incidence and vice versa at grazing incidence, has been described earlier by Gland and coworkers.[61]

In contrast to the rather undefined absorption behavior within the pre-edge region of **2**, the C=C π*-transitions of **3** account for a pronounced linear dichroism better suited for quantitative analysis (Figure 5b) yielding a polar angle of $\alpha = 37° \pm 3°$. An azimuthal angle around $\varphi = 90°$ is extracted under the assumption of a single domain being probed (see SI3-2). It is noted that the anisotropy of the utilized silicon oxide substrates is not considered to play a major role regarding the eventual arrangement of the molecules as film formation takes place exclusively at the water-solvent interface and no further structural transitions occur during or after film transfer. Hence, the reference direction for quantitative analysis of angle dependent spectra is defined through the electric field vector $\vec{E}$ (polarization direction).

In consequence, both oxygen-containing compounds appear to form 2D-extended thin films with a well-defined molecular orientation as deduced from the NEXAFS linear dichroism. As opposed to this, we observe only weak or negligible dichroic effects for thin films of both sulfur-containing *N*-heterotriangulenes **4** and **5** (Figure 4e,f). Especially thin films of **5** appear to be of a rather disordered nature as absorption intensities at specific resonant energies are practically identical for all incidence angles and at numerous spots on the extended film (see SI4 for details). Also, it should be mentioned that if α is close to the magic angle of NEXAFS ($\alpha \approx 54.7°$), no dichroic effects are observed, *i.e.*, the corresponding spectrum would appear the same as the spectrum of a structure with a non-preferred molecular orientation.

Detailed quantitative insights into the crystal structures of fabricated layers of **2** and **3** are derived from selected area electron diffraction (SAED) measurements. The high degree of crystallinity as implied by OM, AFM and NEXAFS can be confirmed via clean electron diffraction patterns for both compounds (Figure 6). The lack of notable Debye-Scherrer rings is indicative of a negligible polycrystalline fraction within the areas examined. Regarding compound **2** (Figure 6a), no loss of crystallinity or change in general crystal structure is observed upon extension from a 1D nanostructure as described by Müllen and coworkers to 2D nanostructured thin films.[42]

Analogous to previous work on this compound,[42] electron diffraction under normal incidence results in highly anisotropic spot patterns due to the arrangement of the columnar stacks along the preferential growth direction. However, from the positions of the main reflections we derive a slightly lower
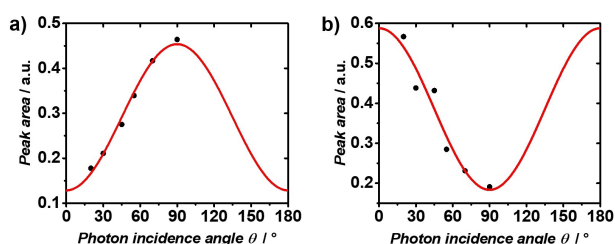

Figure 5. Analysis of distinct dichroic effects and derivation of the respective polar angles, α, for a) compound **2** and b) compound **3**.

Table 1. Characterization overview for all *N*-heterotriangulene thin films. It is noted that the core unit orientation describes the average angle enclosed by the surface normal and the plane of the core unit, *i.e.* 90° – α.

Compound	OM	AFM	RMS [Å]	Core unit orientation	SAED
2	√	√	12.7	~35 ± 3°	√
3	√	√	10.1	53° ± 3°	√
4	√	√	8.2	no unambigious results	✕
5	√	√	6.3	no unambigious results	✕

ChemPhysChem

Articles
doi.org/10.1002/cphc.202100164

**Chemistry
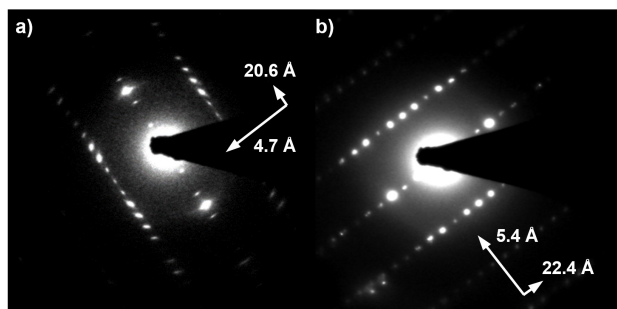Europe**
European Chemical
Societies Publishing

Figure 6. Electron diffraction patterns and deduced in-plane repeating distances of thin films based on a) compound **2**, b) compound **3**.

intercolumnar spacing of only 2.06 nm as compared to 1D structures ($d_{IC} = 2.14$ nm). Similarly, *00 L* reflections parallel to the equatorial plane are assigned to the columnar order and lead to a molecular period of 0.47 nm. Following Müllen and coworkers,[42] *i.e.*, assuming a 45° tilt angle along the columnar stacks, we derive a 0.33 nm π-stacking distance.

Qualitatively, we observe a very similar electron diffraction pattern for **3** (Figure 6b) with unit cell parameters being in the same magnitude as for **2**. For this compound, the intercolumnar spacing is slightly larger (2.24 nm) and within the columnar order, we find the molecular period to be 0.54 nm. Consequently, the π-stacking distance amounts to 0.38 nm assuming a 45° tilt angle along the stacks. It is noticeable that the dimensions of the unit cell differ to a large extent from those derived via X-ray diffraction (XRD) from crystals of compound **3** after synthesis ($a = 6.6$ Å, $b = 12.6$ Å, $c = 17.8$ Å), which will be discussed hereafter. Table 1 summarizes the structure characterization data of all four *N*-heterotriangulene compounds discussed herein.

3. Discussion

In general, the strong interaction of the π-rich *N*-heterotriangulene core units is thought to support long-range supramolecular organization in solution as confirmed within Figure 3. We observe 2D-extended, directional and isotropic thin-film growth to be favored for carbonyl-bridged derivatives exhibiting non-bulky moieties at the aryl *para*-positions. Consistently, the crystal structure of **3**, reveals a short backbone distance between adjacent molecules (Figure 8a, $d_C = 3.44$ Å being the distance from one aromatic ring centroid to the closest aromatic carbon atom of another molecule). As

Figure 7. Geometry optimized *N*-heterotriangulene core units (side view) of carbonyl-bridged (left) and thiocarbonyl-bridged compounds (right).
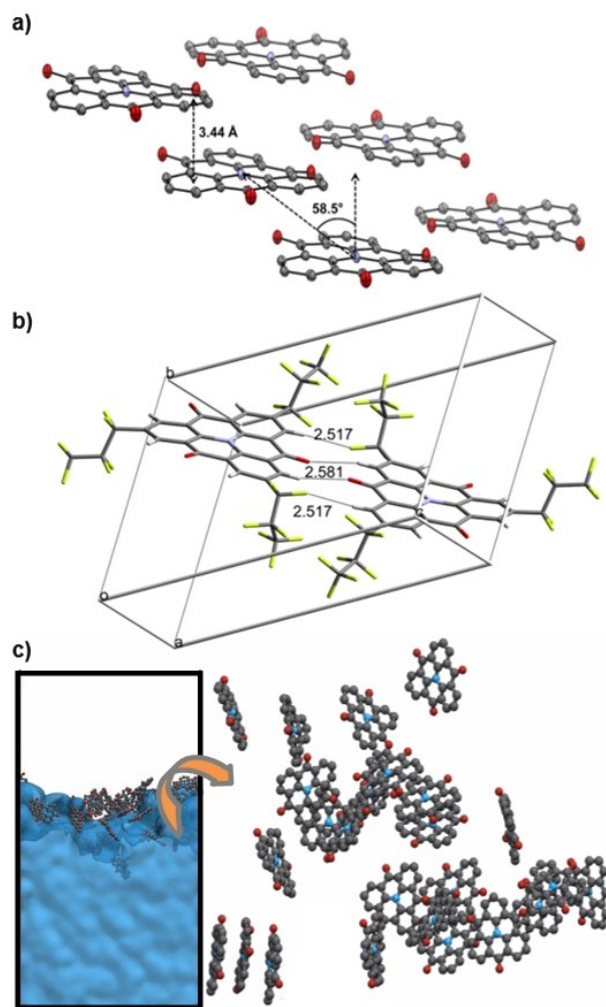

Figure 8. X-ray crystallographic data and MD simulation results for **3**. a) Arrangement of molecules in the bulk showing "stair-like" packing. Indicated are the distance between two planar *N*-heterotriangulene cores and the offset angle. *n*-Perfluoropropyl groups omitted for clarity. b) Top view and intermolecular atomic distances (in Å) of two independent molecules of **3**. Indicated are the short O⋯H_{Ar} and F⋯H_{Ar} interaction distances representing strong hydrogen bonding within the crystal structure. Derived unit cell parameters correspond to $a = 6.6$ Å, $b = 12.6$ Å, $c = 17.8$ Å. c) Arrangement of **3** at a water-vapor interface shown from the side (left) and from above (right, water molecules and n-perfluoropropyl groups omitted for clarity).

observed via NEXAFS, both **4** and **5** appear to lack a distinct preferential orientation potentially due to the larger sulfur atoms at the bridge positions of the backbone. Indeed, quantum mechanical geometry optimizations (see SI7 for details) suggest an angulate core unit for sulfur-containing compounds (Figure 7) due to the increased electron density and additional space demanded at the bridge positions. Hence, the intermolecular distance of the core units is expected to increase for thiocarbonyl-bridged compounds **4** and **5** impeding efficient π-π-stacking to a large extent. As a result, facile, directional self-assembly as observed for carbonyl-bridged counterparts with a flat core structure is considerably hampered.

ChemPhysChem

Articles
doi.org/10.1002/cphc.202100164

Chemistry Europe
European Chemical
Societies Publishing

Additionally, 2D-extended film formation of *N*-heterotriangulenes **S2** and **S3** featuring bulky substituents without acetylene 'spacer' units (as apparent in **5**) at the aryl *para*-positions was not observed to any extent (see SI5 for details). With space-demanding moieties linked directly to the *N*-heterotriangulene core, coplanarity of the aromatic systems is increasingly difficult to achieve due in large part to the adjacent H-atoms. Hence, we anticipate the growth process for latter compounds to be strongly anisotropic as molecules aggregate into elongated one-dimensional fiber structures or needles. For compound **3**, the average alignment of the π-heavy core units can be derived from angle-dependent NEXAFS measurements via data fitting procedures reported in literature (see SI3-2 for details).[49,62–64] Although films of compound **2** do not show a significant NEXAFS dichroism in the core unit related resonances, preferential molecular arrangement can be assumed from the clean SAED pattern and well-defined orientation of the long peripheral alkyl substituents. We expect the orientation of the significant π*-orbitals to be in the region of the magic angle and hence, a core unit tilt angle of ~35.3° from the surface normal. Taking the total film thickness (8.14 nm, derived via AFM) and the maximum molecular extension of the compound (3.79 nm) into account, this leads to 3–4 monolayers as the base film. In contrast, the base film of **3** consists of around 12 monolayers considering the derived molecular parameters, *i.e.*, tilt angle of the backbone from the surface normal (53°), film thickness (17.43 nm) and molecular extension (1.52 nm).

With the sole difference between **2** and **3** being the nature of the respective alkyl substituents, the significant discrepancy in base film thickness and RMS value emphasizes the influence of the side chains at the periphery on the prepared thin film. Adding to the strong π-π-interactions of the core units, the surface normal aligned dodecyl chains of **2** increase the degree of vertical order through extensive VDW interactions and hence, the base film is stable at lower thicknesses. However, the hydrophobicity between the alkyl chains within the topmost layer of **2** and the simultaneously observed mono- and bilayer growth on top of the base film also account for a relatively high RMS roughness value (RMS = 12.7 Å).

On the contrary, shorter fluorinated chains lead to a considerably lower RMS value (RMS = 10.1 Å), but also a higher base film thickness. Indeed, the crystal structure of **3** reveals strong hydrogen bonding between aromatic C—H bonds and CO groups (O···H_{Ar} = 2.52 Å) as well as C—F bonds (F···H_{Ar} = 2.58 Å), which consequently leads to a more shape persistent and homogeneous supramolecular structure (Figure 8b).[65] The hydrophilicity of the perfluorinated substituents and their attractive interaction with the water surface during film formation are found to favor a more lying-down configuration for the core unit as compared to the effect of the hydrophobic dodecyl substituents in compound **2**.

Interestingly, when comparing the SAED pattern of **3** (Figure 6b) with reference data obtained from XRD for bulk crystals (see SI6 for details), we observe significant deviation regarding unit cell parameters. Thus, it might be considered that structure formation on top of the water surface taking place in a confined space, is inherently different as compared to

single crystals obtained from solvent diffusion. To clarify this discordance, molecular dynamics (MD) simulations were performed on the basis of water-vacuum interface mimicking a 6 nm sized liquid slab of 7402 water molecules by means of 2D periodic boundary conditions. Next to the upper slab surface, 58 molecules of **3** were added (at initially randomly chosen positions). From MD simulations for 1 ns at 300 K we characterized the converged state as a 2D liquid-like behavior of the surfactants featuring partial ordering. This demonstrates the preferred columnar stacking motif already in the early stages of film formation (Figure 8c, see SI8-3 for details).

The columnar stacks diverge from the stair-like packing (Figure 8a) as derived via XRD. In fact, the eventual face-to-face orientation of the core units as suggested by MD simulations is reminiscent of the crystal structure of **2** in both 1D fibers[42] and 2D-extended thin films explaining the qualitatively similar electron diffraction patterns of **2** and **3** (Figure 6) to some extent. Hence, with both compounds being capable of forming exceptionally crystalline layered systems, we observe an additional trend towards alike binding motifs for both carbonyl-bridged *N*-heterotriangulenes examined herein. Also, thin-film structures of **2** and **3** emphasize the influence of the 2D-confined liquid surroundings during the growth process. Sufficiently strong π-π interactions as well as the absence of an interacting solid support material are expected to be the main driving force for gradual and consistent self-assembly, resulting in columnar structures, which do not reflect the three-fold symmetry of the mother compound.

Incorporating thin films of **3** and **5** as functional layers into bottom-gate/top-contact OFET devices surprisingly yielded p-type behavior for the realized devices, *i.e.*, current amplification by several orders in magnitude (close to 10^4 at best) was observed with a negative gate voltage applied. It should be noted that thin-film processing in solution under atmospheric conditions commonly disfavors potential n-type semiconducting behavior.[32,33] Hence, our findings emphasize the sensitivity towards diffusion of oxygen and moisture for this compound class and indeed, unexpected hole transporting performance in solution-processed n-type semiconducting structures has been reported before.[66] Recorded charge-carrier mobilities are within the upper regime of 10^{-3} $cm^2V^{-1}s^{-1}$ (see SI9 for details). Although OFETs based on both compounds show unfavorably large threshold voltages higher than −20 V, the switching behavior appeared to be inherently different. With the drain current for **5** increasing instantaneously at gate voltages slightly larger than −20 V and thereby depicting a desirable feature in the field of layered, organic electronics, only gradual amplification was observed above the threshold voltage within semiconducting layers of **3**. OFETs relying on **2** and **4** as functional layers did show neither p-type nor n-type behavior with the long alkyl chains potentially hampering the transport of charge carriers in either direction.

4. Conclusions

In summary, we have successfully prepared 2D-extended thin films of four soluble *N*-heterotriangulene derivatives at the liquid-liquid interface with film thicknesses in the range of 5–20 nm indicative of multilayer systems. Owing to their angulate core unit, compounds exhibiting a thioketone unit at the bridge position lack directional growth behavior and no preferential molecular orientation within realized thin films was observed via NEXAFS. On the contrary, compounds containing a carbonyl moiety were found to form long-range ordered, crystalline layered systems, a fact which was successfully illustrated via AFM, SAED and distinct dichroic effects in angle dependent NEXAFS. For compound **2**, we can confirm a similar crystal structure as in previously reported 1D nanofibers of the same material with the molecular core unit being strongly tilted from and the peripheral substituents aligned with the surface normal.[42] Similarly, thin films of compound **3** show exceptional crystallinity, with the core unit inclined even more and thus, favoring a lying-down configuration. Conveniently, thin films of **3** also illustrate the relevance of the 2D growth conditions as we observe unit cell parameters to diverge from those obtained via XRD. Hence, we may state that both the nature of core and peripheral substituents as well as the dimensionality and preparation method play a vital role in the design of ultrathin crystalline layers. From a preparation standpoint, our work presents a fine tool ensemble for the accurate design and unambiguous structure elucidation of high-quality, 2D *N*-heterotriangulene systems aiming at potential application fields such as layered organic electronics.

Experimental Section

Optical microscopy images were recorded using a Leica DM 4000 M microscope equipped with a Leica DFC 320 camera. AFM images and corresponding height profiles were measured in non-contact mode using a JPK NanoWizard4 microscope. NEXAFS spectra were recorded in partial electron yield mode at the HE-SGM beamline at BESSY II, Berlin, Germany. Electron diffraction patterns were recorded using a Philips CM 30 transmission electron microscope at an acceleration voltage of 300 kV. Charge-transport characteristics of fabricated OFETs were recorded at a Keithley SCS 4200 parameter analyzer under atmospheric conditions. Thin films were prepared via liquid-liquid processing. Beakers were sonicated in acetone and isopropanol for 15 minutes subsequently and rinsed thoroughly with deionized (Millipore) water afterwards. 15 mL of Millipore water were then given into a beaker and solution of the respective *N*-heterotriangulene concentration was added dropwise to form a floating lens on the water surface. Beakers were stored at RT or 278 K respectively until the solvent had evaporated. Resulting thin films were transferred from the water surface onto silicon wafers using a home-made vertical lifting system. Single crystals of **3** suitable for X-ray crystallographic analysis were successfully grown by solvent diffusion of hexanes into a solution of compound **3** in CH_2Cl_2.

Supporting Information

SI1: Compounds synthesis and characterization

SI2: UV-Vis spectra of **2**–**5** and corresponding bandgap calculation from Tauc analysis
SI3: Derivation of the polar and azimuthal angles of **2** and **3** via fitting of NEXAFS spectra
SI4: Additional NEXAFS spectra of **2**, **4** and **5**
SI5: OM images of further *N*-heterotriangulenes with bulky substituents
SI6: X-Ray Crystallographic Data of **3**
SI7: Geometry Optimization of *N*-heterotriangulene core units
SI8: Molecular dynamics simulations of **3**
SI9: OFET preparation and charge-transport parameters for **3** and **5**

Conflict of Interest

The authors declare no conflict of interest.

[1] A. Facchetti, *Chem. Mater.* **2011**, *23*, 733–758.
[2] M. Kaltenbrunner, T. Sekitani, J. Reeder, T. Yokota, K. Kuribara, T. Tokuhara, M. Drack, R. Schwödiauer, I. Graz, S. Bauer-Gogonea, S. Bauer, T. Someya, *Nature* **2013**, *499*, 458–463.
[3] Y. Zang, D. Huang, C.-A. Di, D. Zhu, *Adv. Mater.* **2016**, *28*, 4549–4555.
[4] C. Liao, M. Zhang, M. Y. Yao, T. Hua, L. Li, F. Yan, *Adv. Mater.* **2015**, *27*, 7493–7527.
[5] Y. Yuan, G. Giri, A. L. Ayzner, A. P. Zoombelt, S. C. B. Mannsfeld, J. Chen, D. Nordlund, M. F. Toney, J. Huang, Z. Bao, *Nat. Commun.* **2014**, *5*, 3005.
[6] F. Ebisawa, T. Kurokawa, S. Nara, *J. Appl. Phys.* **1983**, *54*, 3255–3259.
[7] A. Tsumura, H. Koezuka, T. Ando, *Appl. Phys. Lett.* **1986**, *49*, 1210–1212.
[8] R. A. Street, J. E. Northrup, A. Salleo, *Phys. Rev. B* **2005**, *71*, 165202.
[9] N. Kleinhenz, N. Persson, Z. Xue, P. H. Chu, G. Wang, Z. Yuan, M. A. McBride, D. Choi, M. A. Grover, E. Reichmanis, *Chem. Mater.* **2016**, *28*, 3905–3913.
[10] R. Bourguiga, G. Horowitz, F. Garnier, R. Hajlaoui, H. Bouchriha, *Eur. Phys. J. Appl. Phys.* **2002**, *19*, 117–122.
[11] T. Someya, H. E. Katz, A. Gelperin, A. J. Lovinger, A. Dodabalapur, *Appl. Phys. Lett.* **2002**, *81*, 3079–3081.
[12] M. Mas-Torrent, C. Rovira, *Chem. Rev.* **2011**, *111*, 4833–4856.
[13] T. Izawa, E. Miyazaki, K. Takimiya, *Adv. Mater.* **2008**, *20*, 3388–3392.
[14] H. Inokuchi, G. Saito, P. Wu, K. Seki, T. B. Tang, T. Mori, K. Imaeda, T. Enoki, Y. Higuchi, K. Inaka, N. Yasuoka, *Chem. Lett.* **1986**, *15*, 1263–1266.

ChemPhysChem

Articles
doi.org/10.1002/cphc.202100164

Chemistry Europe
European Chemical
Societies Publishing

[15] H. Inokuchi, K. Imaeda, T. Enoki, T. Mori, Y. Maruyama, G. Saito, N. Okada, H. Yamochi, K. Seki, Y. Higuchi, N. Yasuoka, *Nature* **1987**, *329*, 39–40.

[16] C. B. Nielsen, I. McCulloch, *Prog. Polym. Sci.* **2013**, *38*, 2053–2069.

[17] F. Guo, A. Karl, Q.-F. Xue, K. C. Tam, K. Forberich, C. J. Brabec, *Light Sci. Appl.* **2017**, *6*, e17094.

[18] H. Uoyama, K. Goushi, K. Shizu, H. Nomura, C. Adachi, *Nature* **2012**, *492*, 234–238.

[19] K. Takimiya, M. Nakano, H. Sugino, I. Osaka, *Synth. Met.* **2016**, *217*, 68–78.

[20] H. Iino, J.-I. Hanna, *Polym. J.* **2016**, *49*, 23–30.

[21] J. M. Wasikiewicz, L. Abu-Sen, A. B. Horn, J. M. Koelewijn, A. V. S. Parry, J. J. Morrison, S. G. Yeates, *J. Mater. Chem. C* **2016**, *4*, 7309–7315.

[22] J. Li, M. Wang, S. Ren, X. Gao, W. Hong, H. Li, D. Zhu, *J. Mater. Chem.* **2012**, *22*, 10496–10500.

[23] H. A. Becerril, M. E. Roberts, Z. Liu, J. Locklin, Z. Bao, *Adv. Mater.* **2008**, *20*, 2588–2594.

[24] J. Choi, H. Song, N. Kim, F. S. Kim, *Semicond. Sci. Technol.* **2015**, *30*, 064002.

[25] A. R. Brown, C. P. Jarrett, D. M. de Leeuw, M. Matters, *Synth. Met.* **1997**, *88*, 37–55.

[26] Z. Q. Gao, B. X. Mi, G. Z. Xu, Y. Q. Wan, M. L. Gong, K. W. Cheah, C. H. Chen, *Chem. Commun.* **2008**, *1* 117–119.

[27] C. D. Dimitrakopoulos, P. R. L. Malenfant, *Adv. Mater.* **2002**, *14*, 99–117.

[28] Y. Kunugi, K. Takimiya, K. Yamane, K. Yamashita, Y. Aso, T. Otsubo, *Chem. Mater.* **2003**, *15*, 6–7.

[29] Q. Meng, W. Hu, *Phys. Chem. Chem. Phys.* **2012**, *14*, 14152–14164.

[30] Y. Zhao, Y. Guo, Y. Liu, *Adv. Mater.* **2013**, *25*, 5372–5391.

[31] H. Usta, A. Facchetti, T. J. Marks, *Acc. Chem. Res.* **2011**, *44*, 501–510.

[32] J. E. Anthony, A. Facchetti, M. Heeney, S. R. Marder, X. Zhan, *Adv. Mater.* **2010**, *22*, 3876–3892.

[33] X. Gao, Y. Hu, *J. Mater. Chem. C* **2014**, *2*, 3099–3117.

[34] Y. Wang, T. Hasegawa, H. Matsumoto, T. Mori, T. Michinobu, *Adv. Mater.* **2018**, *30*, 1707164.

[35] M. Saito, I. Osaka, Y. Suda, H. Yoshida, K. Takimiya, *Adv. Mater.* **2016**, *28*, 6921–6925.

[36] N. Hammer, T. A. Schaub, U. Meinhardt, M. Kivala, *Chem. Rec.* **2015**, *15*, 1119–1131.

[37] T. A. Schaub, K. Padberg, M. Kivala, *J. Phys. Org. Chem.* **2020**, *33*, e4022.

[38] M. Hirai, N. Tanaka, M. Sakai, S. Yamaguchi, *Chem. Rev.* **2019**, *119*, 8291–8331.

[39] A. Winter, U. S. Schubert, *Mater. Chem. Front.* **2019**, *3*, 2308–2325.

[40] H. Zhang, S. Wang, Y. Li, B. Zhang, C. Du, X. Wan, Y. Chen, *Tetrahedron* **2009**, *65*, 4455–4463.

[41] M. Kivala, W. Pisula, S. Wang, A. Mavrinskiy, J.-P. Gisselbrecht, X. Feng, K. Müllen, *Chem. Eur. J.* **2013**, *19*, 8117–8128.

[42] S. Wang, M. Kivala, I. Lieberwirth, K. Kirchhoff, X. Feng, W. Pisula, K. Müllen, *ChemPhysChem* **2011**, *12*, 1648–1651.

[43] C. Wöll in *Physical and Chemical Aspects of Organic Electronics: From Fundamentals to Functioning Devices*, Wiley-VCH, Bochum, **2009**.

[44] E. Ripaud, D. Demeter, T. Rousseau, E. Boucard-Cétol, M. Allain, R. Po, P. Leriche, J. Roncali, *Dyes Pigm.* **2012**, *95*, 126–133.

[45] W. M. McGregor, D. C. Sherrington, *Chem. Soc. Rev.* **1993**, *22*, 199–204.

[46] C. Xu, P. He, J. Liu, A. Cui, H. Dong, Y. Zhen, W. Chen, W. Hu, *Angew. Chem. Int. Ed. Engl.* **2016**, *55*, 9519–9523.

[47] Q. Wang, F. Yang, Y. Zhang, M. Chen, X. Zhang, S. Lei, R. Li, W. Hu, *J. Am. Chem. Soc.* **2018**, *140*, 5339–5342.

[48] M. M. Nahid, E. Gann, L. Thomsen, C. R. McNeill, *Eur. Polym. J.* **2016**, *81*, 532–554.

[49] J. Stöhr in *NEXAFS spectroscopy*, Springer, New York, **1996**.

[50] O. Dhez, H. Ade, S. G. Urquhart, *J. Electron Spectrosc. Relat. Phenom.* **2003**, *128*, 85–96.

[51] J. Kikuma, B. P. Tonner, *J. Electron Spectrosc. Relat. Phenom.* **1996**, *82*, 53–60.

[52] N. T. Samuel, C.-Y. Lee, L. J. Gamble, D. A. Fischer, D. G. Castner, *J. Electron Spectrosc. Relat. Phenom.* **2006**, *152*, 134–142.

[53] J. MacNaughton, A. Moewes, E. Z. Kurmaev, *J. Phys. Chem. B* **2005**, *109*, 7749–7757.

[54] H. Ade, A. P. Hitchcock, *Polymer* **2008**, *49*, 643–675.

[55] B. Watts, S. Swaraj, D. Nordlund, J. Lüning, H. Ade, *J. Chem. Phys.* **2011**, *134*, 024702.

[56] S. G. Urquhart, H. Ade, *J. Phys. Chem. B* **2002**, *106*, 8531–8538.

[57] N. Haack, G. Ceballos, H. Wende, K. Baberschke, D. Arvanitis, A. L. Ankudinov, J. J. Rehr, *Phys. Rev. Lett.* **2000**, *84*, 614–617.

[58] D. A. Outka, J. Stöhr, J. Rabe, J. D. Swalen, H. H. Rotermund, *Phys. Rev. Lett.* **1987**, *59*, 1321–1324.

[59] J. Fu, S. G. Urquhart, *J. Phys. Chem. A* **2005**, *109*, 11724–11732.

[60] M. Zharnikov, S. Frey, K. Heister, M. Grunze, *J. Electron Spectrosc. Relat. Phenom.* **2002**, *124*, 15–24.

[61] D. G. Castner, K. B. Lewis, D. A. Fischer, B. D. Ratner, J. L. Gland, *Langmuir* **1993**, *9*, 537–542.

[62] F. Zheng, B. N. Park, S. Seo, P. G. Evans, F. J. Himpsel, *J. Chem. Phys.* **2007**, *126*, 154702.

[63] S. Söhnchen, S. Lukas, G. Witte, *J. Chem. Phys.* **2004**, *121*, 525–534.

[64] F.-J. Meyer zu Heringdorf, M. C. Reuter, R. M. Tromp, *Nature* **2001**, *412*, 517–520.

[65] G. A. Jeffrey in *An Introduction to Hydrogen Bonding*, Oxford University Press, New York, **1997**.

[66] Z. Yan, B. Sun, Y. Li, *Chem. Commun.* **2013**, *49*, 3790–3792.